Inorganic Chemistry

Article

pubs.acs.org/IC

A Double Substitution of Mg^{2+}–Si^{4+}/Ge^{4+} for $Al_{(1)}^{3+}$–$Al_{(2)}^{3+}$ in Ce^{3+}-Doped Garnet Phosphor for White LEDs

Mengmeng Shang,[†] Jian Fan,[§] Hongzhou Lian,[†] Yang Zhang,[†,‡] Dongling Geng,[†,‡] and Jun Lin*[,†]

[†]State Key Laboratory of Rare Earth Resource Utilization, Changchun Institute of Applied Chemistry, Chinese Academy of Sciences, Changchun 130022, P. R. China

[‡]Graduate School of the Chinese Academy of Sciences, Beijing 100049, P. R. China

[§]College of Chemical and Environmental Engineering, Shandong University of Science and Technology, Qingdao 266590, P. R. China

Supporting Information

ABSTRACT: The influence of Mg^{2+}–Si^{4+}/Ge^{4+} incorporation into Ce^{3+}-doped $Y_3Al_5O_{12}$ garnet phosphors on the crystal structure and luminescence properties is described in this work. X-ray diffraction with Rietveld refinements, photoluminescence spectra, absolute quantum yield, thermal quenching behavior, and lifetimes were utilized to characterize samples. The introduction of Mg^{2+}–Si^{4+}/Ge^{4+} leads to an obvious red shift of emission wavelength under the excitation of blue light, especially for the series of Mg^{2+}–Si^{4+} substitutions, which is suited for white light-emitting diodes (LEDs) with low color temperatures and good color rendering using only a single phosphor. More interestingly, an additional emission band locating at high-energy was observed with ultraviolet excitation, which is different than previous literature. Under the excitation of ultraviolet, the emission color for the Mg^{2+}–Si^{4+} substitutions can be tuned from yellow-green to blue, which is expected to obtain single-phased phosphors with white emission excited with UV-LED chip. The usual Ce^{3+} emission band at low energy has stronger quenching at high temperatures. The mechanisms for the observed phenomena are discussed.

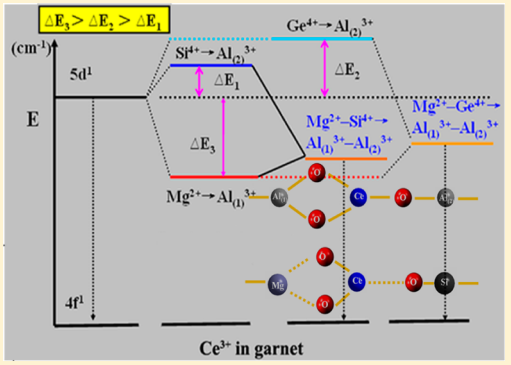

1. INTRODUCTION

Lamps based on phosphor conversion of blue light-emitting diodes (LEDs) are potential candidates for replacing traditional light sources such as fluorescent or incandescent lamps.[1] At present, most of commercial lamps use a yellow-emitting $Y_3Al_5O_{12}$:Ce^{3+} (YAG:Ce^{3+}) garnet-based phosphor and blue LED chip. The efficacies for these phosphor-converted white LEDs can be greater than 80 lm/W for 1 W devices.[2−4] However, the combination of yellow phosphor and blue LED chip gives insufficient color rendering index (CRI), and the produced white light has correlated color temperatures (CCTs) greater than 4500 K due to lack of red spectral composition in the emission spectra of YAG:Ce^{3+} yellow phosphor, which is the limiting factor for such white LEDs applications in general lighting.[5−11]

In the past decade, there have been significant efforts toward shifting the emission spectrum of YAG:Ce^{3+} into the red spectral region, such as codoping with other red-emitting rare-earth ions (Tb^{3+}, Pr^{3+}, Sm^{3+}, etc.) into the YAG host and substituting Y^{3+} by other cations (especially Gd^{3+}).[12,13] However, emission spectra obtained by the above methods do not have the continuous spectral characteristics, and the luminous efficiency is reduced. It is well-known that the position of Ce^{3+} 5d energy levels depends on the nephelauxetic effect (covalency), crystal field splitting, and the Stokes shift.[14,15] Recently, Setlur et al. reported the photoluminescence properties of Si^{4+}–$N^{3−}$-incorporated YAG:Ce^{3+}, which is an important work into red shifting the color point of YAG:Ce^{3+} phosphor.[16] In their work, Si^{4+} replaces Al^{3+} sites in YAG, and $N^{3−}$ is the charge compensating ion. The incorporation of Si^{4+}–$N^{3−}$ into the YAG host lattice leads to a larger crystal field splitting, and the Ce^{3+} emission is strongly red-shifted.

The commercial yellow phosphor host, $Y_3Al_5O_{12}$, belongs to cubic and has garnet-type structure with general stoichimoetric formula of $Y_3Al_{(1)2}Al_{(2)3}O_{12}$, where $Al_{(1)}$ and $Al_{(2)}$ represent the Al sites with octahedral and tetrahedral coordination, respectively. The crystal structure and local coordination surroundings of $Y_3Al_5O_{12}$ are shown in Figure 1. Therefore, the color point of the YAG:Ce^{3+} phosphor can be tailored by varying the crystal field through cation substitutions in the host lattice. In 1981, Robertson et al.[17] first reported that a double substitution of Mg^{2+}–Si^{4+} for $Al_{(1)}^{3+}$–$Al_{(2)}^{3+}$ in YAG host lattice could result in the red shift of emission band. However, the influences of this substitution on the photoluminescence properties (including emission intensity, quantum yield, thermal quenching behavior, etc.) were not studied in detail. To that end, we incorporated Mg^{2+}–Si^{4+} and Mg^{2+}–Ge^{4+} ion pairs into the YAG host lattice for substituting $Al_{(1)}^{3+}$–$Al_{(2)}^{3+}$ sites in the present work and conducted an in-depth and

Received: May 7, 2014
Published: June 27, 2014

   dx.doi.org/10.1021/ic501063j | Inorg. Chem. 2014, 53, 7748−7755

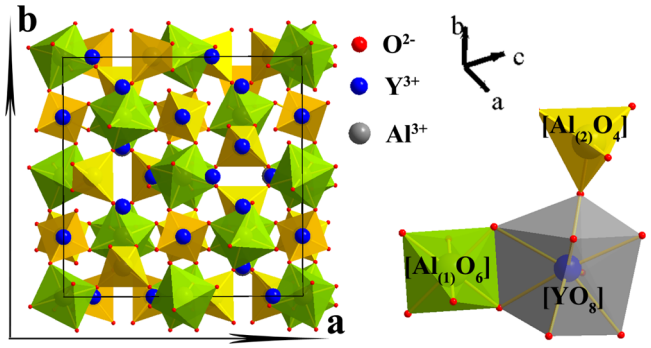

Figure 1. Crystal structure of $Y_3Al_5O_{12}$ viewed along the *c*-axis (left) and the coordination surroundings of Y^{3+} and Al^{3+} cations in the lattice (right).

detailed investigation into the influences of these substitutions on the photoluminescence properties. More interestingly, the new excitation and emission band for all those substitutions were observed when excited with ultraviolet, which is first reported here. The corresponding luminescence mechanisms are proposed in detail in this work.

2. EXPERIMENTAL SECTION

The phosphors with compositions of $Y_3Al_{5-2x}Mg_x(Si/Ge)_xO_{12}:Ce^{3+}$ ($0 \le x \le 2$) were prepared using the high-temperature solid-state reaction method. Note that the doping concentration of Ce^{3+} was fixed at 2 mol % Y^{3+}, namely, $Y_{3-0.06}Al_5O_{12}:0.06Ce^{3+}$ ($x = 0$). Powder phosphor samples were made using mixtures of high-purity Y_2O_3, Al_2O_3, MgO, SiO_2/GeO_2, and CeO_2 fired in air at 1400−1500 °C for 5 h. The appropriate amount of AlF_3 was additionally added as a fluxing agent to improve the efficiency of these phosphors. After that, the samples were reduced at 1200 °C for 3 h in a 10% H_2/90% N_2 gas mixture.

The composition and phase purity of products were studied by X-ray powder diffraction (XRD) measurements using a D8 Focus diffractometer (Bruker) with Cu Kα radiation (λ = 0.154 05 nm). The data were collected over a 2θ range from 10° to 100° at intervals of 0.02° with a counting time of 2 s per step. Crystal structure refinement employed the Rietveld method as implemented in the General Structure Analysis System (GSAS) software suite.[18] High-resolution transmission electron microscopic (HRTEM) images were recorded with a FEI Tecnai G2 S-Twin with a field-emission gun operating at 200 kV and a Gatan multiople CCD camera. Room-temperature photoluminescence (PL) spectra were measured on a Hitachi F-7000 luminescence spectrophotometer equipped with a 150 W xenon lamp as the excitation source. Photoluminescence quantum yields (QY) were measured directly by the absolute PL quantum yield (internal quantum efficiency) measurement system (C9920−02, Hamamatsu Photonics K. K., Japan). The temperature-dependent (200−500 K) PL spectra were obtained on a fluorescence spectrophotometer equipped with a 450 W xenon lamp as the excitation source (Edinburgh Instruments FLSP-920) with a temperature controller. The luminescence decay curves were obtained from a Lecroy Wave Runner 6100 digital osilloscope (1 GHz) using a tunable laser (pulse width = 4 ns; gate = 50 ns) as the excitation (Contimuum Sunlite OPO).

3. RESULTS AND DISCUSSION

3.1. Crystal Structure. Figure 2 presents the X-ray Rietveld refinement results for the $Y_3Al_5O_{12}:Ce^{3+}$ material (x = 0 sample), as well as the $Mg^{2+}-Si^{4+}$ and $Mg^{2+}-Ge^{4+}$ series at x = 1 and 0.4, respectively. The local crystal structures and HRTEM images are also shown in Figure 2. The starting model was built with crystallographic data taken from ISCD-16825 for the structure of $Y_3Al_5O_{12}$. The structural parameters

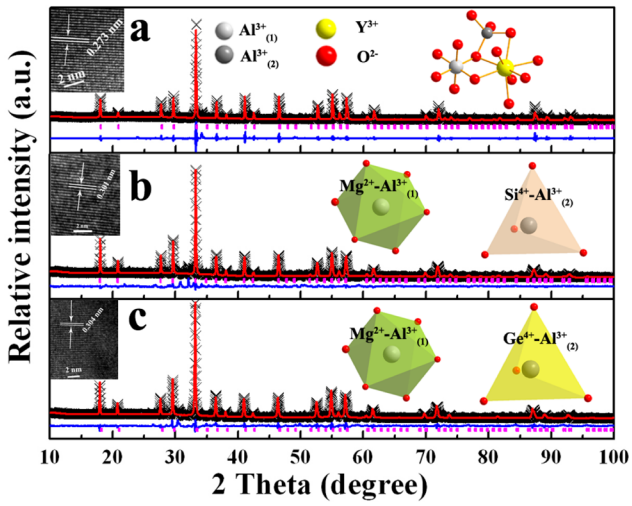

Figure 2. X-ray Rietveld refinements for (a) $Y_3Al_5O_{12}:Ce^{3+}$, (b) $Y_3Al_{5-2x}Mg_xSi_xO_{12}:Ce^{3+}$ (x = 1), and (c) $Y_3Al_{5-2x}Mg_xGe_xO_{12}:Ce^{3+}$ (x = 0.4). The insets are their corresponding HRTEM images.

as determined by Rietveld refinement of powder XRD data are listed in Table S1 (Supporting Information). The refinement confirmed that the single-phase nature of the compound is cubic in space group $Ia\bar{3}d$ and the solid solutions with garnet structure are formed in both series of materials. Microstructures of samples $Y_3Al_5O_{12}:Ce^{3+}$, $Y_3Al_3MgSiO_{12}:Ce^{3+}$ (x = 1), and $Y_3Al_{4.2}Mg_{0.4}Ge_{0.4}O_{12}:Ce^{3+}$ (x = 0.4) were examined using HRTEM shown in the insets of Figure 2. Typical HRTEM images show a very uniform contrast, indicating that these single-phase samples are highly crystalline and without significant defects. The distances between the adjacent fringes for the three samples were estimated to be 0.273 nm, 0.301 nm, 0.304 nm, respectively, corresponding well with the d_{420} spacing of the pure $Y_3Al_5O_{12}$ phase (0.269 nm reported for $Y_3Al_5O_{12}$, JCPDS card no. 79−1891). The trend of increase gradually for d_{420} spacing is due to the expansion of unit cell parameter (see Table S1, Supporting Information). Figures S1 and S2 (Supporting Information) compare the XRD patterns of $Y_3Al_{5-2x}Mg_xSi_xO_{12}:Ce^{3+}$ and $Y_3Al_{5-2x}Mg_xGe_xO_{12}:Ce^{3+}$ ($0 \le x \le 2$) samples with the calculated pattern of $Y_3Al_5O_{12}:Ce^{3+}$ obtained by GSAS refinement. From the patterns, we can conclude that solid solutions with garnet structure can form within a certain range of x value. However, the phase-segregation appears gradually with the increase of x value due to the difference in ionic radius between $Mg^{2+}-Si^{4+}/Ge^{4+}$ and $Al^{3+}-Al^{3+}$. In addition, the synthesized solid solution materials exhibit a slight shift toward lower 2θ angles compared with the reference pattern as the content of $Mg^{2+}-Si^{4+}/Ge^{4+}$ pairs increased. It indicates that the lattice parameter a ($= b = c$) of these materials has expanded. The variations of the lattice parameter in both series, which are obtained from the results of the refinement, are plotted in Figure 3. This could be attributed to the smaller $Al^{3+}_{(1)}$ ions (radius 67.5 pm) in the octahedral sites that were replaced by larger Mg^{2+} ions (radius 86 pm) leading to the expansion of the unit cell in spite of the smaller ionic radius of Si^{4+} (radius 40 pm)/Ge^{4+} (radius 44 pm) than $Al^{3+}_{(2)}$ ions (radius ~53 pm) in the tetrahedral sites.[19,20] Moreover, we also find that the lattice parameter of Ge^{4+} series is larger than that of Si^{4+} series at the same x value. So the x value for Ge^{4+} series (1.0) forming the solid solution is lower than that of the Si^{4+} series (1.4).

dx.doi.org/10.1021/ic501063j | Inorg. Chem. 2014, 53, 7748−7755

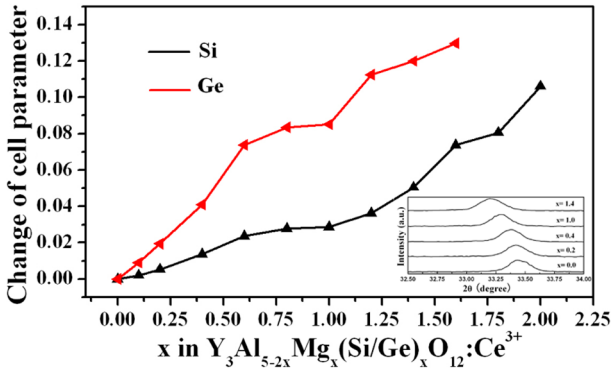

Figure 3. Relative shifts in the lattice parameter a (= b = c) with x in $Y_3Al_{5-2x}Mg_x(Si/Ge)_xO_{12}:Ce^{3+}$. The inset details the evolution of reflections near $2\theta = 33.4°$ for Si^{4+} series, which shift to smaller degree with increasing the x value.

3.2. The Influence of Mg^{2+}–Si^{4+} and Mg^{2+}–Ge^{4+} Pairs Incorporation into YAG:Ce^{3+} Phosphor on the Photoluminescence Properties. Figure S3 (Supporting Information) shows the typical photoluminescence excitation and emission spectra of the as-synthesized YAG:Ce^{3+} phosphor. Being consistent with the reported literature,[20−22] YAG:Ce^{3+} exhibits a yellowish-green emission band ranging from 470 to 650 nm with peak at 528 nm under the 456 nm blue light excitation, which corresponds to the 5d → 4f transition of the Ce^{3+} ions; the excitation spectrum monitored at 528 nm is composed of two broad excitation bands in the regions of 310−370 nm and 390−500 nm, which is due to the transition from the $4f^1$ ground state to the $4f^05d^1$ excited state of Ce^{3+} ions.[23−25] Moreover, under the excitation of the high-energy absorption band at 342 nm, the shape and position of the emission peak do not change obviously as presented by the blue curve in Figure S3 (Supporting Information). The photoluminescence properties for YAG:Ce^{3+} phosphor have been studied widely,[21,26] and further discussion is needless here. Therefore, more attention is paid to the effect induced by Mg^{2+}–Si^{4+}/Ge^{4+} ion pairs incorporation. Figure 4 presents the normalized emission spectra (λ_{ex} = 456 nm) of

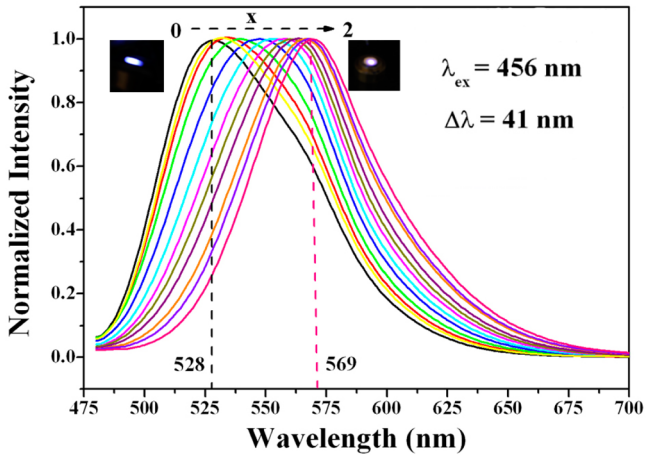

Figure 4. Photoluminescence emission spectra of $Y_3Al_{5-2x}Mg_xSi_xO_{12}:Ce^{3+}$ ($0 \le x \le 2$) solid solutions excited by blue light at 456 nm with different Mg^{2+}–Si^{4+} content. Insets show the luminescence photographs for samples with composition of $x = 0$ and $x = 2$.

$Y_3Al_{5-2x}Mg_xSi_xO_{12}:Ce^{3+}$ samples with different Mg^{2+}–Si^{4+} substituted contents. As shown in Figure 4, the emission spectra show a progressive red shift as x increases in the series of $Y_3Al_{5-2x}Mg_xSi_xO_{12}:Ce^{3+}$ samples, from λ_{em} = 528 nm ($x = 0$) to λ_{em} = 569 nm ($x = 2$) with wavelength offset ($\Delta\lambda$) up to 41 nm. Under the blue light excitation, the emission color varies from cool white light to warm white light as the luminescence photographs recorded with digital single lens reflex camera shown in the insets of Figure 4. With increasing the incorporation content of Mg^{2+}–Si^{4+} ion pairs, the CIE chromaticity coordinates shown in Figure 5 vary from x =

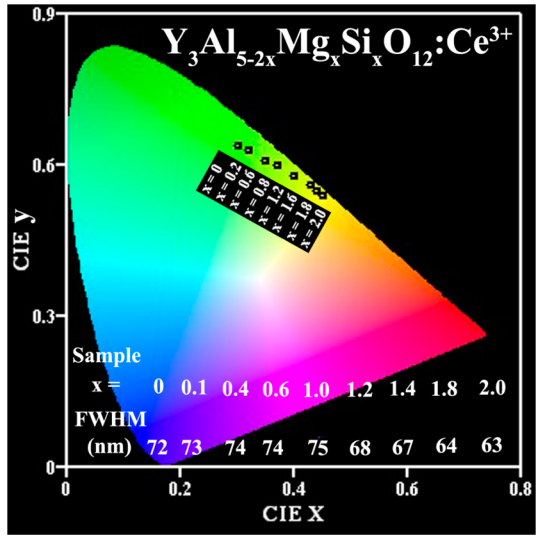

Figure 5. CIE chromaticity coordinates for $Y_3Al_{5-2x}Mg_xSi_xO_{12}:Ce^{3+}$ phosphor series and the fwhm for different x values.

0.30, y = 0.64 (yellowish-green region) to x = 0.43, y = 0.56 (yellow-orange region). The shift in emission wavelength allows for the color properties of a solid-state device to be easily tuned for different applications. The emission band for the Mg^{2+}–Si^{4+} series has greatly red shifted when compared with the yellowish-green emission of the YAG:Ce^{3+}, making them promising candidates for white light emission without an additional red component under the excitation of blue light. Additionally, the full-width at half-maximum (fwhm) of the emission peak calculated by the emission profile slightly broadens from 72 to 75 nm as x increases from 0 to 1.0, which will lead to high color rendering for white LED applications in ambient lighting. However, along with the continuous increase of x, the fwhm narrows obviously, ranging from 75 to 63 nm, which may be due to the garnet structure of the host lattice that has been changed to some degree, and phase segregation appears as the Mg^{2+}–Si^{4+} content increases. Although the phosphors with narrower fwhm are not suitable for lighting, they can be used in the field of background lighting display. The same trend was also observed in the photoluminescence properties of $Y_3Al_{5-2x}Mg_xGe_xO_{12}:Ce^{3+}$ solid solution series as x increased, as shown in Figure 6. However, compared with the Mg^{2+}–Si^{4+} solid solution series, the red shift of emission band for Mg^{2+}–Ge^{4+} solid solution series is much smaller.

Evidently, the emission wavelength of Ce^{3+} depends on both the overall 4f−5d separation and the ligand field splitting of the 5d levels.[22] As the garnet structure for the solid solutions substituted by Mg^{2+}–Si^{4+}/Ge^{4+} is fixed, the 4f−5d separation is

dx.doi.org/10.1021/ic501063j | Inorg. Chem. 2014, 53, 7748−7755

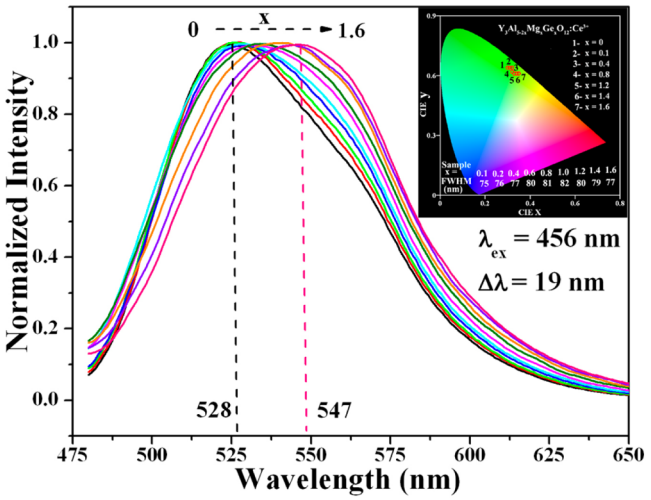

Figure 6. Photoluminescence emission spectra of $Y_3Al_{5-2x}Mg_xGe_xO_{12}:Ce^{3+}$ ($0 \le x \le 1.6$) solid solutions excited by blue light at 456 nm with different $Mg^{2+}-Ge^{4+}$ content. The inset shows the corresponding CIE chromaticity coordinates and the fwhm for different x values.

approximately constant, and the ligand field effect dominates. According to reports by Robertson et al.,[17] crystal field splitting (D_q) can be determined by the following equation:

$$D_q = \frac{1}{6} Ze^2 \frac{r^4}{R^5} \quad (1)$$

where D_q is a measure of the energy level separation, Z is the anion charge, e is the electron charge, r is the radius of the d wavelength, and R is the bond length. The ion radius of Mg^{2+} with 6-fold coordination is larger than that of Al^{3+}, so the ability to attract electrons of Mg^{2+} is poorer. When the $Al^{3+}_{(1)}$ site is substituted by the Mg^{2+} ion, the bond distance between Mg^{2+} and O^{2-} increases, while the bond distance (R_{Ce-O}) between adjacent Ce^{3+} and O^{2-} decreases. According to the above equation, the crystal field strength increases. So the 5d level would be lowered, and the emission peak shifts to longer wavelength (red shift). However, smaller Si^{4+} or Ge^{4+} substituting for $Al^{3+}_{(2)}$ would lead to a longer R_{Ce-O} and decrease the crystal field strength around Ce^{3+} ion, so that the emission wavelength would be blue-shifted. In the $Y_3Al_{5-2x}Mg_xSi_xO_{12}:Ce^{3+}$ and $Y_3Al_{5-2x}Mg_xGe_xO_{12}:Ce^{3+}$ solid solutions, $Mg^{2+}-Si^{4+}/Ge^{4+}$ as ion pairs substituting for $Al^{3+}_{(1)}-Al^{3+}_{(2)}$ are synchronously incorporated into the $Y_3Al_5O_{12}:Ce^{3+}$ host lattice. According to the previous discussion about crystal structure (shown in Figure 1), YO_8 dodecahedrons share the vertex (one O^{2-} ion) with SiO_4 tetrahedron, while YO_8 dodecahedrons share the edge (two O^{2-} ions) with MgO_6 octahedrons. So the augmenter of the crystal field strength arising from Mg^{2+} substitution would dominate, resulting in the red shift of the emission band. Figure 7 shows the schematic energy level diagram for Ce^{3+} in garnets and illustrates the effect of doping $Mg^{2+}-Si^{4+}$ and $Mg^{2+}-Ge^{4+}$ pairs on photoluminescence properties of Ce^{3+} as discussed above. Briefly speaking, the influence of Mg^{2+} (red shift) on the crystal field strength is much greater than that of Si^{4+} (blue shift), leading to the red shift of the emission peak finally.

Figure 8a shows the dependence of the CCT, calculated from the corresponding emission spectrum using a given software, on the content of $Mg^{2+}-Si^{4+}$ and $Mg^{2+}-Ge^{4+}$ ion pairs. It can

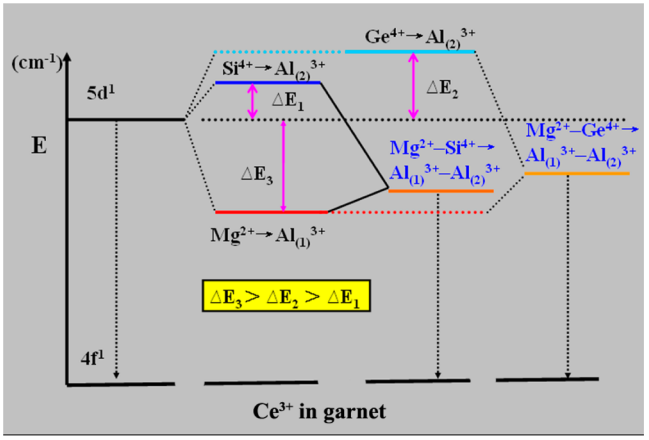

Figure 7. Energy-level diagram showing the lowest-energy ground state and the first excited 5d state of Ce^{3+} in garnet. The energy change for the 5d state is indicated by ΔE.

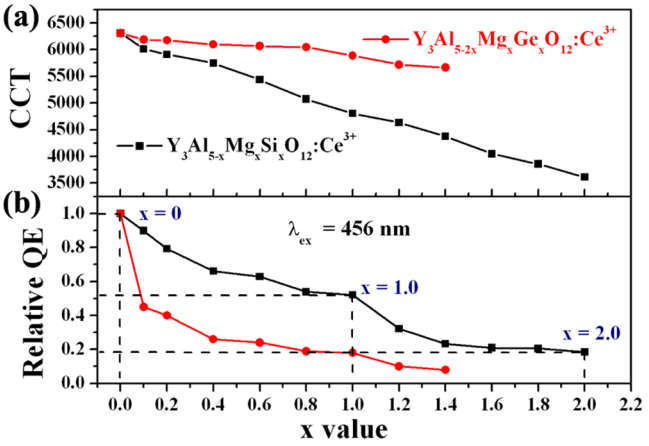

Figure 8. Change of (a) correlated color temperature (CCT) and (b) the relative quantum efficiency (QE) value of $Y_3Al_{5-2x}Mg_x(Si/Ge)_xO_{12}:Ce^{3+}$ samples as a function of the x value.

be concluded that YAG:Ce^{3+} phosphor without $Mg^{2+}-Si^{4+}/Ge^{4+}$ incorporated has higher CCT, which is the limiting factor for its application in white LED. With the content of $Mg^{2+}-Si^{4+}/Ge^{4+}$ ion pairs increasing, the CCT is gradually reduced and can be lower than 4000 K for x = 2 with the $Y_3AlMg_2Si_2O_{12}:Ce^{3+}$ composition. Consistent with their PL spectral properties, the CCT of $Mg^{2+}-Si^{4+}$ series is lower than that of $Mg^{2+}-Ge^{4+}$ series at the same substituted compositions. The quantum efficiency (QE) for all synthesized samples was measured. We define the QE of YAG:Ce^{3+} as 100%, and the relative QE for the substituted samples is shown in Figure 8b. We observe that incorporating $Mg^{2+}-Si^{4+}/Ge^{4+}$ ion pairs into the YAG:Ce^{3+} phosphors causes an obvious drop in QE. At the point of x = 1, the QE of the $Y_3Al_3MgSiO_{12}:Ce^{3+}$ composition was reduced to 50% of the YAG:Ce^{3+} phosphor, and the QE of $Y_3Al_3MgGeO_{12}:Ce^{3+}$ is only 20% of the YAG:Ce^{3+} phosphor. It is well-known that QE for phosphors is closely related to the structure of their matrix compound. Although the incorporation of $Mg^{2+}-Si^{4+}/Ge^{4+}$ into $Y_3Al_5O_{12}$ host lattice does not change the macrostructure of the host, which retains its garnet structure with cubic phase, the microstructure around Ce^{3+} was changed as we discussed above. So the decrease of the QE may be attributed to the distorted crystal lattice after the $Mg^{2+}-Si^{4+}$ substitution. In addition, in the following part

dx.doi.org/10.1021/ic501063j | Inorg. Chem. 2014, 53, 7748−7755

(Section 3.3), we observed that the incorporation of Mg^{2+}–Si^{4+} ion pairs would lead to an additional site occupied by Ce^{3+}, which does not result in the change of the YAG-garnet macrostructure but only changes the microstructure around the Ce^{3+} ions in the host lattice. This additional Ce^{3+} site gave a blue emission band under the UV excitation, which is another reason for the decrease of the QE for the yellow-red emission band. Moreover, the rapid drop in QE for the Ge^{4+} series is most likely due to Ce^{3+} photoionization due to the relatively small band gap of germinate hosts.[27] For example, the Ce^{3+} QE is reduced at higher Ge^{4+} concentrations in other germinate garnets, such as $Lu_2CaMg_2(Si, Ge)_3O_{12}$[28] and $Ca_3Sc_2Ge_3O_{12}$.[29] This luminescence quenching process can be thought of as a metal–metal charge transfer between Ce^{3+} and Ge^{4+}.

The thermal stability is an important factor for ensuring a high efficiency of phosphor-converted devices.[30−32] Figure 9 shows temperature-dependent PL spectra for the Mg^{2+}–Si^{4+} series, which is measured from 200 to 500 K. It can be observed that there is a rapid decline in emission intensity with increasing temperature, and at the same temperature, the higher the x value, the more severe the thermal quenching effect. It is an indication that the thermal quenching of the series for $Y_3Al_{5-2x}Mg_xSi_xO_{12}:Ce^{3+}$ solid solutions is somewhat stronger in comparison to the parent YAG:Ce^{3+} material. The decrease in emission intensities with increasing temperature can be described by thermal quenching at configurational coordinate diagram.[33,34] The excited luminescent center is thermally activated through phonon interaction and then thermally released through the crossing point between the excited state and the ground state in configurational coordinate diagram. This nonraditive transition probability by thermal activation is strongly dependent on temperature, resulting in the decrease of emission intensity. In addition, the peak positions of emission spectra (inset in Figure 9) exhibit a slight red shift with increasing temperature: the peak positions at 200 and 500 K are 581 and 586 nm, respectively. The red-shift behavior can be explained by the Varshini equation for temperature dependence[35]

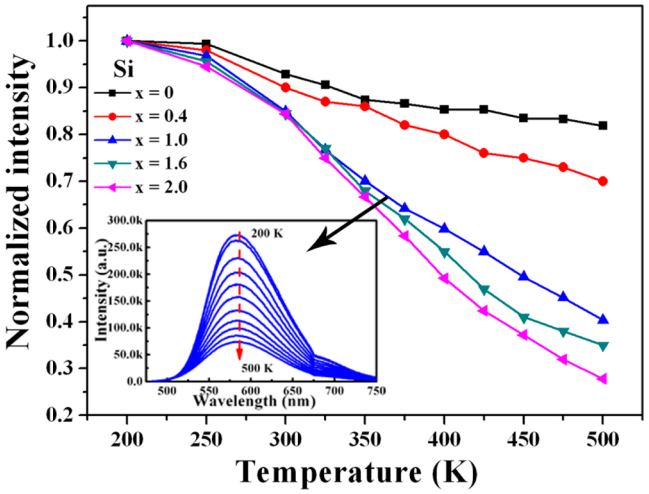

Figure 9. Thermal quenching behavior for photoluminescence $Y_3Al_{5-2x}Mg_xSi_xO_{12}:Ce^{3+}$ samples. The inset shows the temperature-dependent photoluminescence spectra of the representative $Y_3Al_3MgSiO_{12}:Ce^{3+}$ (x = 1.0) sample.

$$E_{(T)} = E_0 - \frac{aT^2}{T + b} \tag{2}$$

where $E_{(T)}$ is the energy difference between excited states and ground states at a temperature T, E_0 is the energy difference at 0 K, and a and b are fitting parameters. At higher temperature, the bond length between a luminescent center and its ligand ions is increased, resulting in the decreased crystal field. Also the symmetry of luminescent center is distorted so that John–Teller effect is dominant. Two causes effect the splitting of degenerate excited state or ground state.[33] It results in the decrease of the transition energy, and the emission peak is red-shifted with an increase in temperature. Quenching temperature ($T_{0.5}$, the temperature at which PL intensity is half of its initial value) is a parameter that characterizes the thermostability of the PL emission intensity. From Figure 9, quenching temperature decreases with increasing x value for Mg^{2+}–Si^{4+} content, which indicates the thermal stability of the solid solutions with $Y_3Al_{5-2x}Mg_xSi_xO_{12}:Ce^{3+}$ composition decreases with x increased. According to the spectral results, the emission peak shifted to red region with increasing x values, which means that the Stokes shift between 4f–5d absorption and 5d–4f emission gradually increases and the quenching activation energy (E_a, energy barrier for thermal quenching) is reduced.[14] So the thermal quenching is more likely to occur. On the other hand, the simplest equation to describe thermal quenching of luminescence intensity $I_{(T)}$ with temperature T is given by[36]

$$I_{(T)} = \frac{I_{(0)}}{1 + \frac{\Gamma_0}{\Gamma_\nu}\exp\left(\frac{-\Delta E}{\kappa_B T}\right)} \tag{3}$$

where Γ_ν is the radiative decay rate of the 5d state of Ce^{3+}, Γ_0 is the attempt rate for thermal quenching, k_B is Boltzmann's constant ($(8.629 \times 10^{-5}$ eV/K), and ΔE is the energy barrier for thermal quenching. The related equation for the decay rate of the 5d state is given by

$$\Gamma(T) = \Gamma_\nu + \Gamma_0 \exp\left(\frac{-\Delta E}{\kappa_B T}\right) \tag{4}$$

The attempt rate Γ_0 has similar magnitude as the maximum phonon frequency (typically 10^{13} Hz corresponding with phonon energies of 1000 cm^{-1}) in compounds. The radiative decay rate of the 5d–4f emission in Ce^{3+} is typically 10^6 Hz. Using these values in eq 3, one obtains

$$\Delta E = \frac{T_{0.5}}{680}\text{eV} \tag{5}$$

as a crude relationship between the quenching temperature $T_{0.5}$ and the energy barrier ΔE. Equation 5 reveals that the higher the Mg^{2+}–Si^{4+} content, the lower the $T_{0.5}$ and the lower the energy barrier for thermal quenching, which is consistent with the effect of the Stokes shift. A similar trend in the thermal quenching behavior for the Mg^{2+}–Ge^{4+} series is observed and not repeated here. It is worth stating that the thermal stability for the Mg^{2+}–Ge^{4+} series is poorer than that of the Mg^{2+}–Si^{4+} series.

Moreover, the coordination environment also influences the PL lifetime through nonradiative relaxation, such as multiphonon decay or energy transfer from activators to the other neighbors.[30,37,38] Figure 10a,b shows the decay profiles of $Y_3Al_{5-2x}Mg_xSi_xO_{12}:Ce^{3+}$ and $Y_3Al_{5-2x}Mg_xGe_xO_{12}:Ce^{3+}$ with different Mg^{2+}–Si^{4+}/Ge^{4+} content, respectively, and Figure

dx.doi.org/10.1021/ic501063j | Inorg. Chem. 2014, 53, 7748−7755

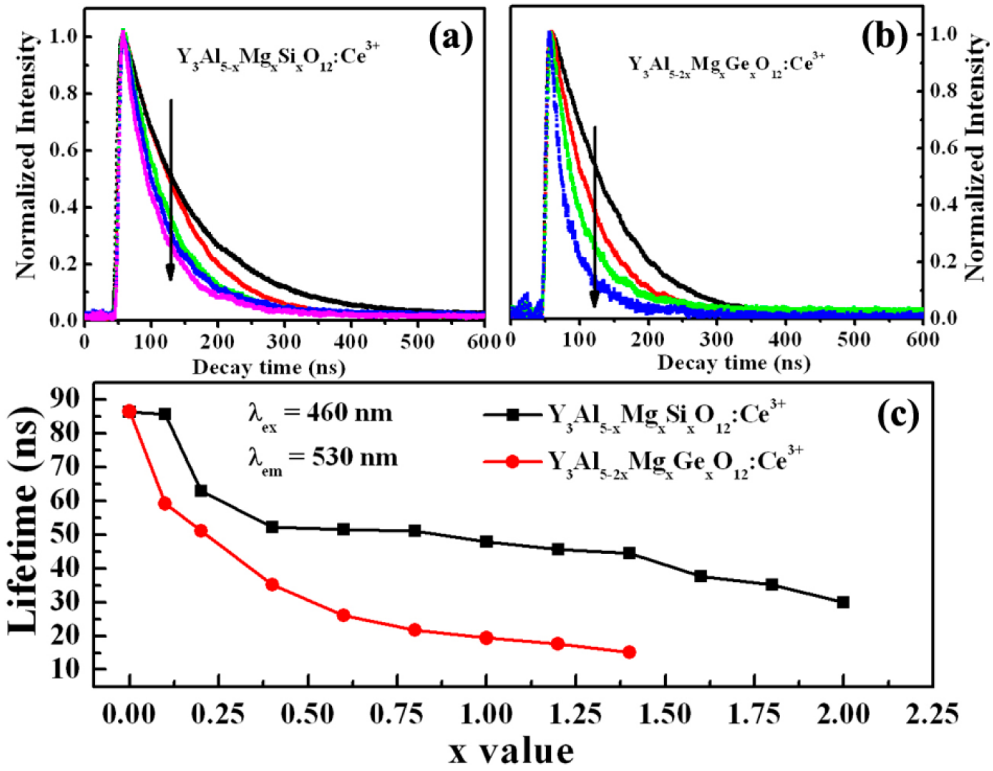

Figure 10. Luminescence of decay profiles for representative (a) $Y_3Al_{5-2x}Mg_xSi_xO_{12}:Ce^{3+}$ (x = 0, 0.4, 0.8, 1.0, 1.4) and (b) $Y_3Al_{5-2x}Mg_xGe_xO_{12}:Ce^{3+}$ (x = 0, 0.4, 0.8, 1.0,); (c) the plots of the fitted lifetimes against x for the $Y_3Al_{5-2x}Mg_x(Si/Ge)_xO_{12}:Ce^{3+}$.

10c gives the corresponding lifetime values excited at a wavelength of 460 nm and monitored with the emission wavelength of 530 nm. The lifetime rapidly decreases in both series with x increased. This trend coincides with the thermal quenching behavior discussed above. The trends in the PL and nonradiative processes (such as thermal quenching and PL decay behaviors) reflect that the Ce^{3+} activators are sensitive to the local sites.

As discussed above, the incorporation of $Mg^{2+}-Si^{4+}/Ge^{4+}$ ion pairs into garnet host lattice leads to the lower energy of 5d excited state of Ce^{3+} compared to typical garnets and an obvious red shift of the Ce^{3+} emission band, which lowers the CCTs and improves the CRI. Unfortunately, the low-energy Ce^{3+} ions in the modulating host structure with strong crystal field have stronger luminescent thermal quenching and decrease of the absolute QE versus typical Ce^{3+} ions in garnets. In practical terms, this could affect the lamp efficacy and color depending on the LED lamp design and operating conditions.

3.3. The Photoluminescence Properties of the Solid Solutions with $Y_3Al_{5-2x}Mg_xSi_xO_{12}:Ce^{3+}$ Composition ($0 \leq x \leq 1.4$) Excited with Ultraviolet. The above results and discussions demonstrate the influence of incorporation of $Mg^{2+}-Si^{4+}/Ge^{4+}$ into YAG:Ce^{3+} host lattice on the photoluminescence properties of Ce^{3+} ion under the excitation with 460 nm blue light. However, in our present work, an interesting luminescence phenomenon was observed when all the solid solution samples were excited by ultraviolet. Figure 11a shows the variation of PL excitation spectra for $Y_3Al_{5-2x}Mg_xSi_xO_{12}:Ce^{3+}$ samples with different $Mg^{2+}-Si^{4+}$ content in the wavelength range of 250−375 nm (viz., the ultraviolet region). It can be observed that an additional absorption band in the range of 250−330 nm occurs gradually with increasing x value. Accordingly, under the excitation of

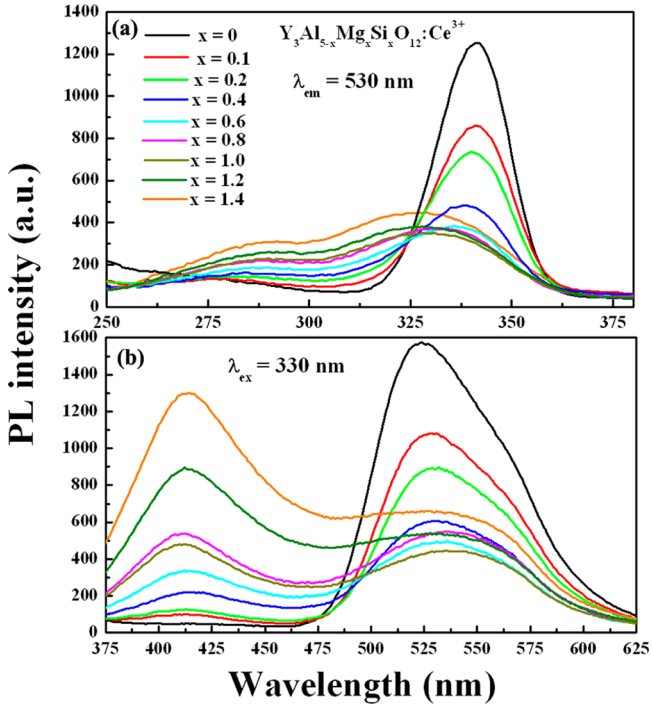

Figure 11. Photoluminescence excitation (a) and emission (b) spectra of $Y_3Al_{5-2x}Mg_xSi_xO_{12}:Ce^{3+}$ samples excited with 330 nm wavelength and monitored with 530 nm wavelength.

ultraviolet at 330 nm, the YAG:Ce^{3+} sample (Figure 11b, black line) only shows one emission peak at 530 nm similar to that excited with blue light at 460 nm. However, an additional emission band with maximum at about 410 nm appears when incorporation of $Mg^{2+}-Si^{4+}$ into the host lattice was

dx.doi.org/10.1021/ic501063j | Inorg. Chem. 2014, 53, 7748−7755

accomplished. It is well-known that the Ce^{3+} emission should be composed of a double band in view of the splitting of its ground state, with the energy difference of about 2000 cm^{-1} with this splitting between the $^2F_{7/2}$ and $^2F_{5/2}$ levels. However, the energy difference between 410 and 530 nm is about 5522 cm^{-1}, which is far from 2000 cm^{-1}. Therefore, this additional emission band cannot be ascribed to the ground-state splitting of the single Ce^{3+} emission center. So the profile changes in the emission and excitation spectra are attributed to the presence of two different Ce^{3+} luminescence centers in the present study. However, in the garnet-YAG host, there is only one type of Y^{3+} site for Ce^{3+} substitution. As the analysis about crystal field in the part of PL properties showed (emission intensity, thermal quenching behavior, etc.), the local crystal structure around Ce^{3+} changed with the incorporation of Mg^{2+}−Si^{4+} ion pairs into the YAG-based phosphor. So we can assume that the incorporation of Mg^{2+}−Si^{4+} ion pairs would lead to an additional site occupied by Ce^{3+}, which does not result in the change of the YAG-garnet macrostructure and only change the microstructure around Ce^{3+} ions in the host lattice. So the phase still remains a single phase as demonstrated by XRD Rietveld analysis in Figure 2. The systematical model for neighboring-cation substitution is shown in Figure S4 (Supporting Information). Central Ce^{3+} ion surrounded with MgO_6 octahedron and SiO_4 tetrahedron would allow the emission at 410 nm.

In addition, with increasing x value, the intensity of the emission peak at 410 nm becomes stronger and that of the emission peak at 530 nm becomes weaker. So the emission color can be tuned from yellowish-green to blue region under the excitation of 330 nm, as shown in Figure S5 (Supporting Information). On the basis of the tunable emission properties, a white light emission would be obtained in the single-phased $Y_3Al_{5-2x}Mg_xSi_xO_{12}$ host through codoping another activator ion (such as Mn^{2+}, Sm^{3+}, Pr^{3+}) with red emission under the excitation of ultraviolet.[39] The corresponding part will be studied in another work in detail.

4. CONCLUSIONS

In summary, the luminescence of YAG:Ce^{3+} phosphor with Mg^{2+}−Si^{4+} and Mg^{2+}−Ge^{4+} replacing $Al^{3+}_{(1)}$−$Al^{3+}_{(2)}$ on octahedral and tetrahedral sites is discussed and analyzed. The incorporation of Mg^{2+}−Si^{4+}/Ge^{4+} ion pairs into garnet host lattice leads to the lower energy of 5d excited state of Ce^{3+} compared to typical garnets. Under the excitation of blue light at 460 nm, the emission band exhibits an obvious red shift, which lowers the CCTs and improves the CRI. Unfortunately, there is the potential limitation that the low-energy Ce^{3+} ions in the modulating host structure with strong crystal field have stronger luminescent thermal-quenching versus typical Ce^{3+} ions in garnets. In practical terms, this could affect the lamp efficacy and color depending on the LED lamp design and operating conditions. Interestingly, excited by ultraviolet at 330 nm, an additional emission band in the range of 375−500 nm is observed, and the emission color for the Mg^{2+}−Si^{4+} substitutions can be tuned from yellow-green to blue, which is expected to obtain single-phased phosphors with white emission excited with UV−LED chip.

■ ASSOCIATED CONTENT

Supporting Information

Structure parameters for $Y_3Al_5O_{12}:Ce^{3+}$, $Y_3Al_{5-2x}Mg_xSi_xO12:Ce^{3+}$ (x = 1), and $Y_3Al_{5-2x}Mg_xGe_xO12:Ce^{3+}$ (x = 0.4) (Table S1); XRD patterns for $Y_3Al_{5-2x}Mg_xSi_xO_{12}:Ce^{3+}$ samples (Figure S1); XRD patterns for $Y_3Al_{5-2x}Mg_xGe_xO_{12}:Ce^{3+}$ samples (Figure S2); photoluminescence excitation and emission spectra of YAG:Ce^{3+} (Figure S3); local structural coordination of $Y_3Al_5O_{12}:Ce^{3+}$ $Y_3Al_{5-2x}Mg_xSi_xO_{12}:Ce^{3+}$ (Figure S4); CIE chromaticity diagram (Figure S5). These materials are available free of charge via the Internet at http://pubs.acs.org.

■ AUTHOR INFORMATION

Corresponding Author

*E-mail: jlin@ciac.ac.cn.

Notes

The authors declare no competing financial interest.

■ ACKNOWLEDGMENTS

This work is financially supported by the National Natural Science Foundation of China (NSFC 51332008, 51372243, 21221061), the Joint Funds of the National Natural Science Foundation of China and Guangdong Province (U1301242), and the National Basic Research Program of China (2010CB327704, 2014CB643803).

■ REFERENCES

(1) Lozano, G.; Louwers, D. J.; Rodríguez, S. R. K.; Murai, S.; Jansen, O. T. A.; Verschuuren, M. A.; Gomez Rivas, J. *Light: Sci. Appl.* **2013**, *2*, e66.

(2) Narukawa, Y.; Narita, J.; Sakamoto, T.; Deguchi, K.; Yamada, T.; Mukai, T. *Jpn. J. Appl. Phys.* **2006**, *45*, L1084.

(3) Schubert, E. F.; Kim, J. K. *Science* **2005**, *308*, 1274−1278.

(4) Wickleder, C. *Angew. Chem., Int. Ed.* **2011**, *50*, 806−808.

(5) Höppe, H. A. *Angew. Chem.* **2009**, *121*, 3626−3236.

(6) Huang, C. H.; Chen, T. M. *Inorg. Chem.* **2011**, *50*, 5725−5730.

(7) Roushan, M.; Zhang, X.; Li, J. *Angew. Chem.* **2012**, *124*, 451−454.

(8) Shin, J. S.; Kim, H. J.; Jeong, Y. K.; Kim, K. B.; Kang, J. G. *Mater. Chem. Phys.* **2011**, *126*, 591−595.

(9) Huang, W. Y.; Yoshimura, F.; Ueda, K.; Shimomura, Y.; Sheu, H. S.; Chan, T. S.; Greer, H. F.; Zhou, W.; Hu, S. F.; Liu, R. S.; Attfield, J. P. *Angew. Chem., Int. Ed.* **2013**, *52*, 8102−8106.

(10) Li, X. F.; Budai, J. D.; Liu, F.; Howe, J. Y.; Zhang, J. H.; Wang, X. J.; Gu, Z. J.; Sun, C. J.; Meltzer, R. S.; Pan, Z. W. *Light: Sci. Appl.* **2013**, *2*, e50−e58.

(11) Park, W. B.; Singh, S. P.; Sohn, K. S. *J. Am. Chem. Soc.* **2014**, *136*, 2363−2373.

(12) Jang, H. S.; Im, W. B.; Lee, D. C.; Jeon, D. Y.; Kim, S. S. *J. Lumin.* **2007**, *126*, 371−377.

(13) Pan, Y.; Wu, M.; Su, Q. *J. Phys. Chem. Solids* **2004**, *65*, 845−850.

(14) Blasse, G.; Grabmaier, B. C. *Luminescent Materials;* Springer-Verlag: Berlin, Germany, 1994.

(15) Wang, Z. L.; Chan, H. L. W.; Li, H. L.; Hao, J. H. *Appl. Phys. Lett.* **2008**, *93*, 141106.

(16) Setlur, A. A.; Heward, W. J.; Hannah, M. E.; Happek, U. *Chem. Mater.* **2008**, *20*, 6277−6283.

(17) Robertson, J. M.; Tol, M. W. V.; Smits, W. H.; Heyene, J. P. H. *Philips J. Res.* **1981**, *36*, 15−30.

(18) Larson, A. C.; Dreele, R. B. V. *General Structure Analysis System (GSAS);* Technical Report for the Los Alamos National Laboratory: Los Alamos, NM, 2004; pp 86−748

(19) Liu, C. S.; Shu, W. B.; Tung, M. J.; Ke, M. Y. *J. Appl. Phys.* **1990**, *67*, 5506.

(20) Katelnikovas, A.; Bettentrup, H.; Uhlich, D.; Sakirzanovas, S.; Jüstel, T.; Kareiva, A. *J. Lumin.* **2009**, *129*, 1356−1361.

(21) Lin, Y. S.; Tseng, Y. H.; Liu, R. S.; Chan, J. C. C. *J. Electrochem. Soc.* **2007**, *154*, P16−P19.

(22) Dorenbos, P. *J. Lumin.* **2000**, *91*, 155−176.

(23) Zhang, X.; Zhou, L.; Pang, Q.; Shi, J.; Gong, M. *J. Phys. Chem. C* **2014**, *118*, 7591−7598.
(24) Thomas, S.; Oró-Solé, J.; Glorieux, B.; Jubera, V.; Buissette, V.; Le Mercier, T.; Garcia, A.; Fuertes, A. *J. Mater. Chem.* **2012**, *22*, 23913−23920.
(25) Ghosh, P.; Kar, A.; Patra, A. *Nanoscale* **2010**, *2*, 1196−1202.
(26) Wu, J. L.; Gundiah, G.; Cheetham, A. K. *Chem. Phys. Lett.* **2007**, *441*, 250−254.
(27) Blasse, G.; Schipper, W.; Hamelink, J. J. *Inorg. Chim. Acta* **1991**, *189*, 77−80.
(28) Setlur, A. A.; Heward, W. J.; Gao, Y.; Srivastava, A. M.; Chandran, R. G.; Shankar, M. V. *Chem. Mater.* **2006**, *18*, 3314−3322.
(29) Pinelli, S.; Bigotta, S.; Toncelli, A.; Tonelli, M.; Cavalli, E.; Bovero, E. *Opt. Mater.* **2004**, *25*, 91−99.
(30) Wang, S. S.; Chen, W. T.; Li, Y.; Wang, J.; Sheu, H. S.; Liu, R. S. *J. Am. Chem. Soc.* **2013**, *135*, 12504−12507.
(31) Yeh, C. W.; Chen, W. T.; Liu, R. S.; Hu, S. F.; Sheu, H. S.; Chen, J. M.; Hintzen, H. T. *J. Am. Chem. Soc.* **2012**, *134*, 14108−14117.
(32) Li, Y. Q.; de With, G.; Hintzen, H. T. *J. Solid State Chem.* **2008**, *181*, 515−524.
(33) Shionoya, S.; Yen, W. M. *Phosphor Handbook;* CRC Press: Boca Raton, FL, 1998.
(34) Kim, J. S.; Park, Y. H.; Kim, S. M.; Choi, J. C.; Park, H. L. *Solid State Commun.* **2005**, *133*, 445−448.
(35) Varshini, Y. P. *Physica* **1967**, *34*, 149−154.
(36) Dorenbos, P. *J. Phys.: Condens. Matter* **2005**, *17*, 8103−8111.
(37) Layne, C. B.; Lowdermilk, W. H.; Weber, M. *J. Phys. Rev. B* **1977**, *16*, 10−20.
(38) Xu, W.; Wang, Y.; Bai, X.; Dong, B.; Liu, Q.; Chen, J.; Song, H. *J. Phys. Chem. C* **2010**, *114*, 14018−14024.
(39) Shang, M.; Li, C.; Lin, J. *Chem. Soc. Rev.* **2014**, *43*, 1372−1386.

dx.doi.org/10.1021/ic501063j | *Inorg. Chem.* 2014, 53, 7748−7755